

STRUCTURAL CONSTRAINED VIRTUAL HISTOLOGY STAINING FOR HUMAN CORONARY IMAGING USING DEEP LEARNING

Xueshen Li¹, Hongshan Liu¹, Xiaoyu Song³, Brigitta C. Brott², Silvio H. Litovsky², Yu Gan¹

¹Department of Biomedical Engineering, Stevens Institute of Technology, Hoboken, USA

²School of Medicine, The University of Alabama at Birmingham, Birmingham, USA

³The Icahn School of Medicine at Mount Sinai, New York, USA

ABSTRACT

Histopathological analysis is crucial in artery characterization for coronary artery disease (CAD). However, histology requires an invasive and time-consuming process. In this paper, we propose to generate virtual histology staining using Optical Coherence Tomography (OCT) images to enable real-time histological visualization. We develop a deep learning network, namely Coronary-GAN, to transfer coronary OCT images to virtual histology images. With a special consideration on the structural constraints in coronary OCT images, our method achieves better image generation performance than the conventional GAN-based method. The experimental results indicate that Coronary-GAN generates virtual histology images that are similar to real histology images, revealing the human coronary layers.

Index Terms— Virtual histology, Coronary artery disease, Optical coherence tomography, Deep learning

1. INTRODUCTION

Coronary artery disease (CAD) is the third leading cause of mortality worldwide and is associated with 17.8 million deaths annually [1]. Apart from mortality, CAD can lead to symptoms involving angina, shortness of breath, heart attack, heart failure, and depression [2]. The morbidity and implications of CAD emphasize the importance of appropriate diagnosis and management. During percutaneous coronary intervention (PCI), a procedure to treat CAD, a stent is placed to open and keep open narrowed arteries. There is a significant need to improve coronary imaging to guide cardiac care.

One valuable direction is to add histopathological visualization on real-time OCT imaging. Currently, histopathological analysis relies upon an off-line evaluation that requires postmortem evaluation. As an invasive and time-consuming process, histopathology involves fixation of tissues and preparation of thin stained sections followed by microscopic imaging. Multiple reagents are required to process histopathology and may introduce irreversible effects on tissue imaging. The process commonly takes a few hours to several days. It is thus

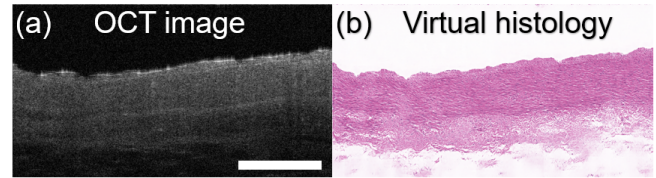


Fig. 1. (a) An example OCT image of a human coronary sample. The scale bar represents 1mm. (b) The virtual histology images that are generated from the example OCT image in (a). The virtual staining process can be done in real-time. The virtual histology image can help in interpreting OCT images.

not available for real-time analysis for tissue characterization of coronary arteries during PCI.

Optical coherence tomography (OCT) is capable of resolving coronary tissue structures [3]. It has been considered an optimal imaging system to assess plaques prior to stenting to ensure successful stent deployment, and to assess vascular response to interventions [4, 5]. However, real-time interpretation of OCT images requires extensive training and prior knowledge and is not at the detailed analytic level as histopathological analysis.

Therefore, there is a movement to generate virtual histology images from OCT images [6]. An example of generating virtual histology images from OCT images for human coronary is shown in Figure 1. Generative Adversarial Networks (GANs), e.g., Pix2Pix GAN, have been developed for virtual histology generation. However, such method requires a pixel-wisely paired OCT and H&E image dataset. Generating the pixel-wisely paired dataset requires a substantial amount of effort, including encasing samples in fluorescent gel, photo-belching, and manually fine alignment, during pre-processing, imaging, and post-processing of the samples [6]. Moreover, the Pix2Pix GAN is trained from the pixel-wisely paired dataset, without considering high-level structural information. It is thus not optimized for virtual staining biological samples which has unique structural patterns.

In this paper, we develop a deep learning network, namely Coronary-GAN, to generate virtual histology images from human coronary OCT images. Our Coronary-GAN is optimized for human coronary samples by incorporating the

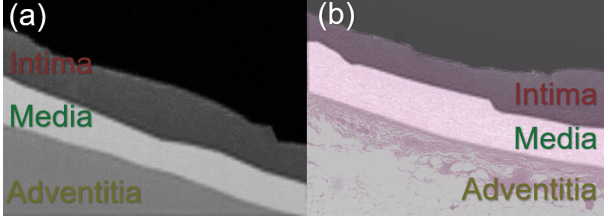


Fig. 2. Representative examples of (a) a labeled OCT image and (b) a labeled H&E images. The intima, media, and adventitia are labeled. The OCT image and H&E image are not pixel-wisely paired.

structural information of the coronary. In summary, the proposed method has the following contributions:

(1) We proposed a generative method to produce colorful virtual stain coronary structures from gray-scale human OCT images using deep learning.

(2) We proposed a Coronary-GAN, which does not require a pixel-wisely paired dataset of OCT and H&E images. The proposed method significantly alleviates the effort for generating the dataset in comparison with existing methods.

2. METHOD

2.1. OCT and H&E data acquisition

Human coronary samples were collected from the School of Medicine at the University of Alabama at Birmingham (UAB). Specimens were imaged via a commercial OCT system (Thorlabs Ganymede, Newton, NJ) [7]. A total of 285 OCT volumes were collected from 23 specimens with an imaging depth of 2.56 mm. The width of the images ranged from 2 mm to 4 mm depending on the actual sample size. Among all the volumes, the pixel size was $2 \mu\text{m} \times 2 \mu\text{m}$ within a B-scan. Samples were processed for Hematoxylin and Eosin (H&E) histology after imaging.

2.2. Generation of human coronary structural database

The human coronary consists of three layers, namely intima, media, and adventitia (from the inner part to the outer part). We labeled the three-layer structure in both OCT and H&E images. An example of labeled OCT and H&E images are shown in Figure 2.

2.3. Design of Coronary-GAN

2.3.1. Network architecture

Details of the Coronary-GAN are shown in Figure 3. The Coronary-GAN consists of a Cycle-GAN network and a coronary structure network. $G_{O \rightarrow H}$ transfers images from OCT domain to histology domain; $G_{H \rightarrow O}$ transfers images from the histology domain to OCT domain. The coronary structure network ensures the structural information of samples

can be encoded and decoded by $G_{O \rightarrow H}$ and $G_{H \rightarrow O}$ respectively. Thus, the virtual staining network is optimized for human coronary samples by learning coronary structural information. The Coronary-GAN does not require a pixel-wisely labeled OCT and H&E dataset.

2.3.2. Loss function

The loss function L of Coronary-GAN consists of four types, which are adversarial loss L_{adv} , cycle-consistency loss L_{cycle} , embedding loss $L_{embedding}$, and coronary structural loss $L_{coronary}$.

$$\begin{aligned}
 L(G_{O \rightarrow H}, G_{H \rightarrow O}, D_H, D_O, G_{O \rightarrow H}^C, G_{H \rightarrow O}^C) \\
 = L_{adv}(G_{O \rightarrow H}, D_H) + L_{adv}(G_{H \rightarrow O}, D_O) \\
 + \alpha L_{cycle}(G_{O \rightarrow H}, G_{H \rightarrow O}) + \beta L_{embedding}(G_{O \rightarrow H}, G_{H \rightarrow O}) \\
 + \gamma L_{coronary}(G_{O \rightarrow H}^C, G_{H \rightarrow O}^C)
 \end{aligned} \tag{1}$$

The L_{adv} and L_{cycle} are described in [8], while α , β , and γ are hyper-parameters. Symbols O and H stand for OCT and Histology images respectively. $G_{O \rightarrow H}$ and $G_{H \rightarrow O}$ are two generators that generate virtual histology images from OCT images and virtual OCT images from histology images respectively. D_H is the discriminator for histology images and D_O is the discriminator for OCT images. $G_{O \rightarrow H}^C$ and $G_{H \rightarrow O}^C$ are the coronary structure networks.

We enforce the structural constraint of human coronary samples by developing an embedding loss function and a coronary structural loss function. In our design, the encoders $G_{O \rightarrow H}^{en}$ and $G_{H \rightarrow O}^{en}$ extract the embedding information of the coronary samples from corresponding OCT and H&E images. Then the decoders $G_{O \rightarrow H}^{de}$ and $G_{H \rightarrow O}^{de}$ perform virtual staining and virtual OCT scanning. We design the $L_{embedding}$ term, minimizing the differences between the embeddings of two generators using L1-norm.

$$\begin{aligned}
 L_{embedding} = \mathbb{E}_H[\|G_{H \rightarrow O}^{en}(G_{O \rightarrow H}(O)) - G_{O \rightarrow H}(O)\|_1] \\
 + \mathbb{E}_O[\|G_{O \rightarrow H}^{en}(G_{H \rightarrow O}(H)) - G_{H \rightarrow O}(H)\|_1]
 \end{aligned} \tag{2}$$

$G_{O \rightarrow H}^C$ and $G_{H \rightarrow O}^C$ predict the pixel-wise segmentation of the feature map acquired by coronary structure mapping of embeddings of encoders. The training of coronary structure networks is supervised by the human coronary structural database using cross-entropy loss terms.

$$\begin{aligned}
 L_{coronary} = \mathbb{E}_H[-N_H^{-1} \sum_{n=1}^{N_H} \sum_{c=1}^C y_H^{n,c} \log(G_{O \rightarrow H}^C(O))] \\
 + \mathbb{E}_O[-N_O^{-1} \sum_{n=1}^{N_O} \sum_{c=1}^C y_O^{n,c} \log(G_{H \rightarrow O}^C(H))]
 \end{aligned} \tag{3}$$

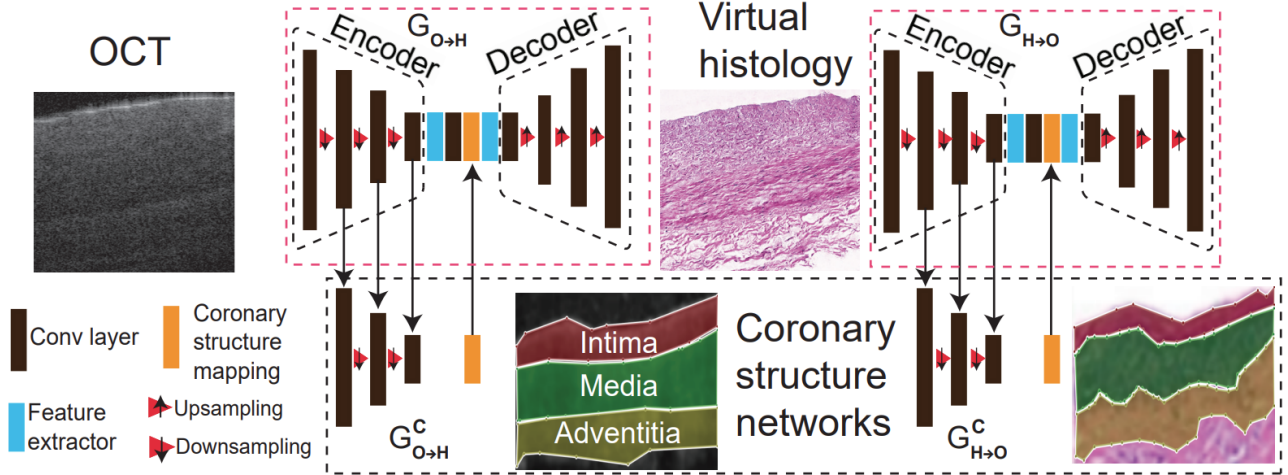


Fig. 3. Scheme of the proposed Coronary-GAN. The Coronary-GAN consists of two generators. Each generator has an encoder-decoder structure. The Coronary-GAN contains a coronary structure network, which segments the three layer structure of human coronary samples.

N_H and N_O stand for the number of pixels in the embeddings acquired from histology and OCT images respectively. y_H and y_O are the labels from the human coronary database for histology and OCT images respectively. C stands for the number of categories of the coronary layers ($c=3$). We aim to solve the following minmax optimization problem:

$$G_{O \rightarrow H}^*, G_{H \rightarrow O}^* = \arg \min \max L(G_{O \rightarrow H}, G_{H \rightarrow O}, D_H, D_O, G_{O \rightarrow H}^C, G_{H \rightarrow O}^C) \quad (4)$$

3. EXPERIMENTAL DESIGN AND RESULTS

3.1. Experimental dataset

From the 285 OCT volumes, we use 104 OCT images and 104 H&E images that reveal intima, media, and adventitia for training and testing. We randomized 52 OCT images and 52 H&E images for training. The other images are used as testing set. The human coronary database were created for the training purpose. The OCT and H&E images in the training set are divided into non-overlap patches with a size of 288×288 . We randomly flip the patches from left to right for data augmentation. The training set contains 1926 OCT image patches and 1926 H&E image patches.

3.2. Network implementation

We implement the Coronary-GAN (shown in Figure 3) using PyTorch. For the encoders, we adopt 3 convolution layers with a stride of 2; for decoders, we adopt 3 transpose convolution layers also with a stride of 2. The feature extractor consists of 5 residual blocks as described in [9]. We use a convolution layer with a stride of 1 to perform coronary structure

mapping. The $G_{O \rightarrow H}$ takes 1 color channel for input and outputs 3 color channels; the $G_{H \rightarrow O}$ takes 3 color channels and outputs 1 color channel. We follow the discriminator design in [8].

3.3. Evaluation setup and metrics

3.3.1. Network training details

The pixel values of OCT and H&E images were scaled to $[0, 1]$. The batch size was 16. The learning rate was initialized as 10^{-4} , followed by a linearly decaying decay for every 2 epochs. α , β , and γ were set to 10, 5, and 5 respectively. In total, the networks were trained 10,000 epochs to ensure convergence. The experiments were carried out in parallel on 2 RTX A6000 GPUs.

3.3.2. Quantitative evaluation metrics

We measure the similarity from pairs of virtual histology and real histology images using Perceptual Hash Value (PHV). This metric has been used in evaluating the quality of virtual histology images [10].

$$PHV = \frac{1}{N} \sum_{n=1}^{n=N} H[|avg(F_i(\hat{H}))_n - avg(F_i(H))_n| - T] \quad (5)$$

The PHV takes advantage of a pre-trained Resnet-101 network. H and \hat{H} represent the real histology and virtual histology images. $F_i(\cdot)$ stands for the feature maps that are generated from i_{th} layer of the Resnet. N is the total channel number of extracted features after pooling. $avg(\cdot)_n$ stands for n^{th} channel after average pooling operation. $H[\cdot]$ is the unit step function and T is a predefined threshold.

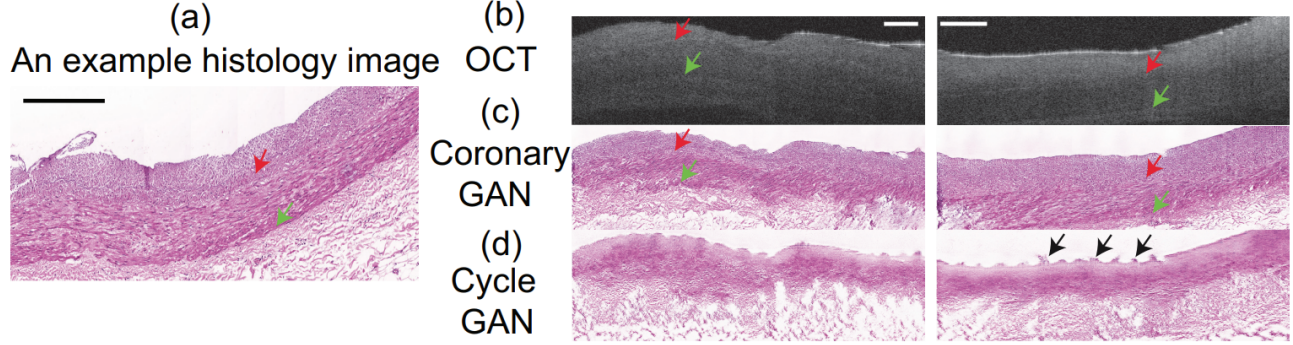


Fig. 4. The visual inspection of two representative OCT images and corresponding virtual histology images. (a) An example H&E stained histology image for reference. (b) Representative OCT images. (c) Virtual histology images generated by Coronary-GAN. (d) Virtual histology images generated by Cycle-GAN. The red arrows indicate the interface between intima and media; the green arrows indicate the interface between intima and adventitia. The black arrows indicate artifacts generated by Cycle-GAN. The scale bars represent $200\mu\text{m}$.

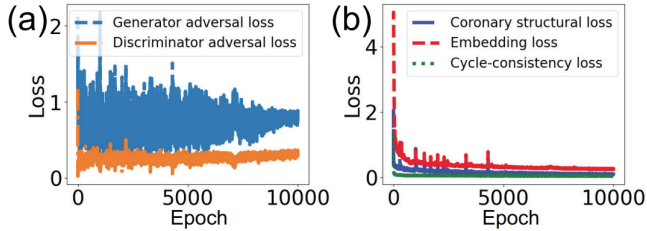


Fig. 5. Plot of loss functions during training of Coronary-GAN over 10,000 epochs. (a) Adversarial loss for generators and discriminators. (b) Cycle-consistency loss, embedding loss, and coronary structural loss.

3.4. Results

3.4.1. Network convergence

We trained the Coronary-GAN for 10,000 epochs. The plots of loss functions are shown in Figure 5. Within 10,000 epochs of training, the Coronary-GAN converges for each loss term.

3.4.2. Coronary-GAN provides better quantitative scores than Cycle-GAN

As suggested in [10], we observe the PHV scores calculated using $i = 1$, $i = 2$, and $i = 3$. The resulting PHV scores are named as PHV_1, PHV_2, and PHV_3 respectively. The T is set to 0.005. The results are reported in Table 2. Comparing to the Cycle-GAN, Coronary-GAN generates virtual histology images that are more similar to the real histology images, which is confirmed by multiple variants of PHV scores.

3.4.3. Coronary-GAN reveals human coronary structure

Two representative OCT images and their corresponding virtual histology images are shown in Figure 4. The virtual histology images generated by Coronary-GAN are capable of

Table 1. The PHV scores calculated using $i = 1$ (PHV_1), $i = 2$ (PHV_2), and $i = 3$ (PHV_3).

Method	Metric		
	PHV_1	PHV_2	PHV_3
Cycle-GAN	55.989	51.389	49.996
Coronary-GAN	61.561	61.308	56.714

revealing the intima, media, adventitia layers, and their interfaces. The virtual histology images generated by Coronary-GAN is capable of providing visually similar images to the example histology image in Figure 4(a). On the contrary, the vanilla Cycle-GAN model fails to characterize layered structure in virtual histology. The performance of Cycle-GAN is substantially deteriorated when virtually staining the media and adventitia layers. Without incorporating structural information of human coronary, the Cycle-GAN can only use pixel intensities to perform virtual staining. The OCT signal attenuation over the sample depth will gradually decrease the pixel intensities, which explains the deteriorated performance of virtual staining media and adventitia layers that are deeper in depth. Moreover, the Cycle-GAN is prone to artifacts due to the lack of structural constrain.

4. CONCLUSIONS

We have developed a virtual staining network, namely Coronary-GAN, for human coronary samples using OCT images. Our Coronary-GAN is optimized for virtually staining human coronary OCT images by incorporating structural constraints. In future, we plan to improve the inference speed of Coronary-GAN, enabling real-time virtual staining. The proposed Coronary-GAN is promising for assisting the diagnosis of CAD by providing real-time, color-channel histology information using OCT images.

5. COMPLIANCE WITH ETHICAL STANDARDS

The human coronary autopsy specimens were de-identified and not considered as human subjects, in compliance with the UAB at Birmingham’s Institutional Review Board (IRB).

6. ACKNOWLEDGMENTS

This work was supported in part by National Science Foundation (CRII-1948540), New Jersey Health Foundation, the National Center for Advancing Translational Research of the National Institutes of Health under award number UL1TR003096.

7. REFERENCES

- [1] Rachel Hajar, “Risk factors for coronary artery disease: historical perspectives,” *Heart views: the official journal of the Gulf Heart Association*, vol. 18, no. 3, pp. 109, 2017.
- [2] F. Lespérance and N. Frasure-Smith, “Depression in patients with cardiac disease: a practical review,” *Journal of psychosomatic research*, vol. 48, no. 4-5, pp. 379–391, 2000.
- [3] Guillermo J. Tearney et al., “Consensus standards for acquisition, measurement, and reporting of intravascular optical coherence tomography studies: A report from the international working group for intravascular optical coherence tomography standardization and validation,” *Journal of the American College of Cardiology*, vol. 59, no. 12, pp. 1058–1072, 2012.
- [4] William Wijns, Junya Shite, Michael R Jones, Stephen W-L Lee, Matthew J Price, Franco Fabbicchi, Emanuele Barbato, Takashi Akasaka, Hiram Bezerra, and David Holmes, “Optical coherence tomography imaging during percutaneous coronary intervention impacts physician decision-making: Illumien i study,” *European heart journal*, vol. 36, no. 47, pp. 3346–3355, 2015.
- [5] Daniel A Jones, Krishnaraj S Rathod, Sudheer Koganti, Stephen Hamshere, Zoe Astroulakis, Pitt Lim, Alexander Sirker, Constantinos O’Mahony, Ajay K Jain, Charles J Knight, et al., “Angiography alone versus angiography plus optical coherence tomography to guide percutaneous coronary intervention: outcomes from the pan-london pci cohort,” *JACC: Cardiovascular Interventions*, vol. 11, no. 14, pp. 1313–1321, 2018.
- [6] Yonatan Winetraub et al., “Oct2hist: Non-invasive virtual biopsy using optical coherence tomography,” *medRxiv*, 2021.
- [7] Xueshen Li et al., “Multi-scale reconstruction of under-sampled spectral-spatial oct data for coronary imaging using deep learning,” *IEEE Transactions on Biomedical Engineering*, pp. 1–1, 2022.
- [8] Jun-Yan Zhu et al., “Unpaired image-to-image translation using cycle-consistent adversarial networks,” in *2017 IEEE International Conference on Computer Vision (ICCV)*, 2017, pp. 2242–2251.
- [9] Kaiming He et al., “Deep residual learning for image recognition,” *2016 IEEE Conference on Computer Vision and Pattern Recognition (CVPR)*, pp. 770–778, 2016.
- [10] Shuting Liu, Baochang Zhang, Yiqing Liu, Anjia Han, Huijuan Shi, Tian Guan, and Yonghong He, “Unpaired stain transfer using pathology-consistent constrained generative adversarial networks,” *IEEE transactions on medical imaging*, vol. 40, no. 8, pp. 1977–1989, 2021.